ANSTO Detection and Imaging

A CONDENSED OVERVIEW OF SUB-GEV HADRONIC PHYSICS IN GEANT4

JEREMY M. C. BROWN, DAVID BOARDMAN AND ALISON FLYNN

11/08/2022

CONTENTS

1. EXECUTIVE SUMMARY

This technical report provides a condensed overview of the underlying physics processes of transport, interaction, and production of sub-GeV hadronic particles in Geant4. The report was developed and funded under Project Arrangement 10256 in collaboration with the Defence Science and Technology Group of the Australian Department of Defence. The material contained in this report provides a complementing resource to the Geant4 Physics Reference Manual (G4PRM) for novice to intermediate user of the Monte Carlo toolkit. The authors acknowledge that this condensed overview draws heavily on the past work of the Geant4 Collaboration (G4Collab) and publications outlined in Section 9 (References).

2. INTRODUCTION/BACKGROUND INFORMATION

The Geant4 toolkit for the simulation of the passage of particles through matter is the result of a worldwide collaboration that has spanned 25+ years [1]. Of the available Monte Carlo radiation transport modelling toolkits Geant4 [2-5] is the most popular in use due to its flexible nature and wide array of different physics transport models. However, this flexibility and extensive physics library comes at the cost of ease of use and transparency in the underlying physics processes in use during radiation transport. This document aims to provide a condensed overview of the underlying physics processes of transport, interaction, and production of sub-GeV hadronic particles in Geant4.

3. A CONDENSED OVERVIEW OF SUB-GEV HADRONIC PHYSICS IN GEANT4

Geant4 separates the majority of it's physics processes into two primary classifications: electromagnetic and hadronic. Electromagnetic (EM) physics processes refer to interaction processes between particles and bound electrons/electronic atomic fields of atoms and materials. Whereas hadronic physics processes are defined to loosely cover any reaction which can produce hadrons in its final state (i.e., neutrons, fission fragments, unstable isotopes). Under this definition hadronic physics processes include purely hadronic interactions, lepton- and gamma-induced nuclear reactions, and radioactive decay. The following outlines the available sub-GeV hadronic physics cross-section datasets and models available in Geant4 version 10.7 via separation into 5 key subtopics: 1) hadron physics cross-section data, 2) inelastic hadronic physics processes/models, 3) radioactive decay, 4) low energy neutron (> 20 MeV) processes, and 5) gamma-nuclear and lepto-nuclear.

4. HADRONIC PHYSICS CROSS-SECTION DATA

Total, inelastic, and elastic cross-sections for hadron–nucleus, and nucleus–nucleus reactions are provided in Geant4 which cover energies up to, and above, 1 GeV [4]. Coulomb cross-sections are implemented within EM physics processes as single or multiple scatterings of charged particles, so the main Coulomb term is excluded from hadron cross-sections. Ideally an interface between electromagnetic and strong amplitudes should be implemented to account for hadronic physics cross-section data, but to date this has been ignored for the main models [5].

4.1. HADRON-NUCLEON CROSS-SECTIONS

Hadron-nucleon cross-section datasets within Geant4 are based on parameterisations of the extensive cross-sectional data tables collated by the "Particle Data Group" in PDG-2016 [6]. Both total and elastic cross-sections are parameterised for protons, anti-protons, pions, and kaons. For positively charged projectiles a Coulomb barrier factor is applied, whereas for negatively charged particles with kinetic energy less then 100 keV in the laboratory frame the cross-section is set to a constant value. Hyperons, charmed and bottom mesons, and baryons implement a scaling from proton and pion cross-sections.

4.2. NEUTRON-NUCLEUS CROSS-SECTIONS

Neutron cross-section data for elastic, inelastic, capture, and fission processes below 20 MeV are available within the HP models which were derived from the Evaluated Nuclear Structure Data File (ENDF/B-VI) evaluated data library [7]. A parallel set of neutron cross-sections optimised for fast access, with lower accuracy sub-20 MeV and a larger energy range, for all target nuclei is contained in the G4PARTICLEXS2.1 based on Barashenkov cross-section interpolations [8, 9].This data set is used for neutron cross-sections in the default and majority of other reference Physics Lists.

Both neutron cross-section datasets are treated as point-wise cross-sections [5]. This has been done to increase computational efficiency and explicitly include all neutron nuclear resonances in the form of point-like cross-sections (rather than in the form of parametrisations). Through this approach the effective error due to linear interpolation between adjacent data points is smaller than a few percent. In the case of fission and inelastic scattering, point-wise semi-inclusive cross-sections are also used in order to decide on the active channel for an individual interaction.

4.3. OTHER HADRON-NUCLEUS CROSS-SECTIONS

For sub-GeV protons and pions a special combination of cross-sections from the Barashenkov interpolations is implemented in Geant4 [8, 9]. This approach has been shown to be both computationally efficient, and accurate with respect to available experimental data for various target nuclei [4, 5]. For all other sub-GeV hadrons and ions, Geant4 implements a cross-section data set based on Gribovs corrected Galuber model. The simplified Glauber model cross-sections assume a Gaussian-distributed nucleus *A* composed of point-like nucleons *N*, that for an incident hadron/ion *h* [10, 11]:

$$\sigma_{tot}^{hA} = 2\pi R(A)^2 ln[1 + \frac{A\sigma_{tot}^{hN}}{2\pi R(A)^2}],\ \sigma_{in}^{hA} = \pi R(A)^2 ln[1 + \frac{A\sigma_{tot}^{hN}}{\pi R(A)^2}],$$

$$\sigma_{el}^{hA} = \sigma_{tot}^{hA} - \sigma_{in}^{hA}$$

where *R(A)* is the radius of the nucleus, and σ_{tot}^{hA}, σ_{in}^{hA}, and σ_{el}^{hA} are the total, incoherent and elastic cross-sections respectively. This approach reduces the number of free parameters down to two fundamental values: the nucleus radius (*R(A)*) and sum of total nucleon cross-sections for a given hadron/ion ($A\sigma_{tot}^{hN}$). When possible PDG-2016 [6] and parameterising datasets are used for $A\sigma_{tot}^{hN}$, otherwise the sum of total nucleon cross-sections for a given hadron/ion is calculated by:

$$A\sigma_{tot}^{hN} = N_p\sigma_{tot}^{hp} + N_n\sigma_{tot}^{hn}$$

where N_p is the number of protons, N_n is the number of neutrons, σ_{tot}^{hp} is the total cross-section of an individual proton, and σ_{tot}^{hn} is the total cross-section of an individual neutron. For the nuclear radius *R(A)*, it is parameterised for A ≤ 50 as:

$$R(A) = f(A)(A^{1/3} - A^{-1/3})$$

with *f(A)* = 1.26 *fm* for A ≤ 15, *f(A)* = 1.19 *fm* for 16 ≤ A ≤ 20, *f(A)* = 1.12 *fm* for 21 ≤ A ≤ 30, and , *f(A)* = 1.1 *fm* for 31 ≤ A ≤ 50 [5]. And when A > 50:

$$R(A) = f(A)(A^{0.27})$$

with *f(A)* = 1.0 *fm* [5].

4.4. NUCLEUS-NUCLEUS CROSS-SECTIONS

For the simulation of nucleus-nucleus interactions, it is important to separate the potential cross-sections in three different categories to maximise computational efficiency: total cross-section (σ_T), elastic cross-section (σ_{el}), and inelastic (or total reaction) cross-section (σ_{in}). Because nuclei are charged, the total and elastic cross-sections can be considered infinite due to Coulomb interactions [5]. However, both these cross-sections are effectively limited due to the impact of atomic screening between the two nuclei associated with either partially or full occupied atomic orbitals. This interaction between the incident nuclei and atomic electrons leads to a small-angle scattering which can be ignored in a first approximation for hadronic processes (see EM physics models for ion transport in [5]). Thus, inelastic (or total reaction) cross-sections are the most important ones as they have the most significant impact for hadronic physics interactions [4].

Above 1 GeV the electromagnetic dissociation (EMD) between nuclei becomes dominant, especially for the collisions of heavy nuclei. At low and intermediate energies EMD does not play an essential role, while the nuclear break-up and multi-particle productions dominate. From geometrical arguments, at low energies the total reaction cross-sections of a projectile-target system is proportional to the area "seen" by the projectile [12-14]:

$$\sigma_{\mathrm{pt}} = \pi r_0^2 (A_p^{1/3} + A_t^{1/3} - b_0)^2$$

where A_p and A_t are the mass numbers of the projectile and the target respectively, b_0 is the overlap or transparency parameter, and r_0 is the constant of proportionality in the expression for the geometrical nuclear radius $r_i = r_0 A_i^{1/3}$. Within the low energy range b_0 and r_0 can be considered energy independent. In order to extend the parameterization to the intermediate energy range, effects related to the Coulomb barrier of the projectile-target system need to be accounted for:

$$\sigma_{pt} = \pi R_{int}^2 (1 - B/E_{CMS})$$

where R_{int} is composed of two parametrised terms, one energy dependent and one independent, $B = Z_p Z_t e^2 / r_C (A_p^{1/3} + A_t^{1/3})$ is the Coulomb barrier of the projectile–target system, and E_{CMS} is centre-of-mass system energy [4]. Shen's parameterizations [15] are implemented within all Geant4 reference physics lists.

5. INELASTIC HADRONIC PHYSICS PROCESSES/MODELS (SUB-GEV)

Inelastic hadronic interactions of particles within Geant4 are some of the most complicated processes that the toolkit supports. Below the sub-GeV energy range, it is not possible for a single model to describe all the physics encountered in a simulation. A typical sequence of reactions may begin with a high energy hadron–nucleon collision within a nucleus, followed by the propagation of the secondaries of the collision through the nuclear medium, followed by the de-excitation of the remnant nucleus and its evaporation of particles until it reaches the ground state. If any "semi-stable" daughter radionuclide exists, their lifetime is sampled and then their decay products are propagated throughout the defined environment. The following will outline the relevant processes and major physics models for this sequence of reactions in the sub-GeV energy range that is presented in Figure 1.

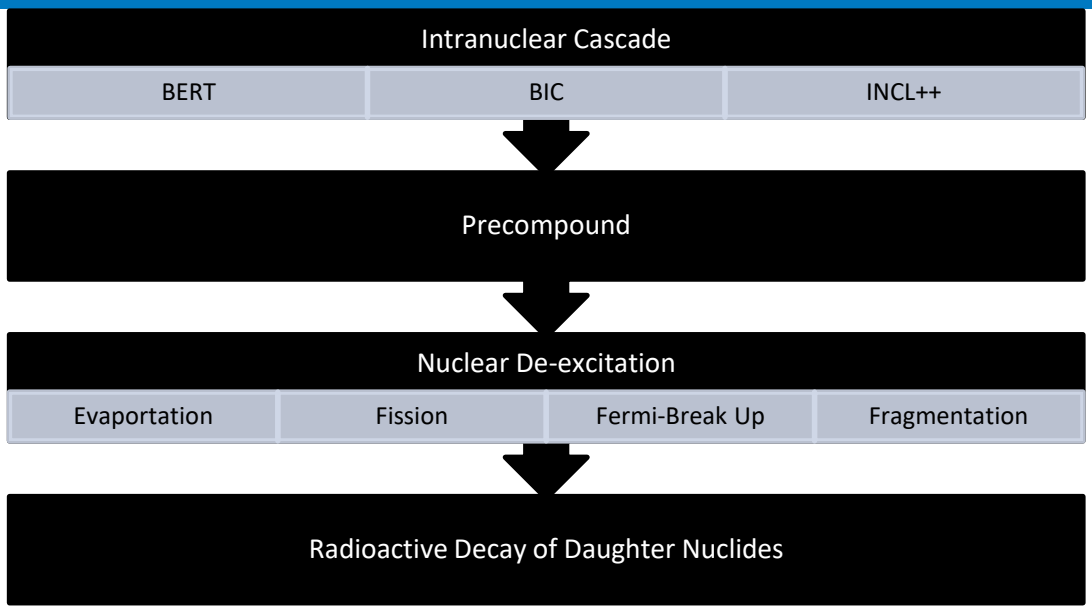

Figure 1. Hadronic physics inelastic interaction workflow

5.1. INTRANUCLEAR CASCADE

Three major intranuclear cascade models are offered in Geant4: Bertini, Binary Intranuclear Cascade (BIC) and INCL++. The following provides an overview of each and outline their connection to the next step in the sequence of reactions.

5.1.1. BERTINI

The Bertini intranuclear cascade model is valid for p, n, π, K, Λ, Σ, Ξ, Ω and γ projectiles with incident energies between 0 and 15 GeV [16]. It is also valid for captured μ− and Σ−, and cascades initiated by high energy muons and electrons. Although this model has its own precompound and deexcitation code, an option exists to implement the native Geant4 precompound and deexcitation modules.

At the core of the Geant4 Bertini model is the concept of the intranuclear cascade of hadrons and nucleons produced through a series of interactions within the nucleus. It is essentially a classical model solving on average the Boltzmann equation for the transport of a particle through a “gas” of nucleons. The nuclear medium may be considered as a gas if the effective nucleon size is small and there are few collisions [5, 16].

To account for the continuously changing density distribution of nuclear matter within a nucleus, the Bertini model approximates the target nucleus as a set of concentric shells of constant density (maximum of six shells) [5, 16]. A cascade is generated when an incident particle interacts with individual protons and/or neutrons in the nucleus, producing a number of different secondary particles. These secondaries can then interact with other protons and neutrons to produce further secondary particles with energies consistent with the individual interactions. Every secondary is propagated through the nucleus, interacting in turn until the last secondaries either escape the nucleus or stop and are absorbed. At this point the residual nucleus is de-excited using the pre-equilibrium and evaporation models. Clusters of nucleons within the initial nucleus are not generally considered, except in the case of pion absorption which requires dinucleons [5, 16].

When all cascade particles have either left or been trapped in the nucleus, the Bertini built-in or native Geant4 nuclear deexcitation codes take over. There is no specific energy at which this occurs, but it corresponds roughly to a system (not a secondary) energy of 200 MeV [16].

Secondaries from the cascade with energies below the nuclear potential are trapped or stopped in the nucleus. These particles are not placed in the final state particle list but are eventually decayed or recombined with the nucleus in the pre-equilibrium phase [5, 16]. The particles destined to recombine from a collection of particle–hole states are described by the Griffin exciton model [17, 18]. These states subsequently deexcite using parameterized level densities which are functions of Z and A. Particle emission from this process is assumed to be isotropic in the rest frame of the exciton system.

Following this stage, the nucleus is further de-excited by Fermi breakup for nuclei with A < 12 (see below for more detail on the Fermi breakup model). All other nuclei undergo equilibrium evaporation via the Dostrovsky et al.'s [19, 20] implementation of the Weisskopf statistical model [21]. For some heavy nuclei (A > 100) fission may be performed [5, 16]. The relative probabilities of the evaporation of nucleons, light ions (d, ^{3}He, t, α), and fission are used to implement competition between these processes as highlighted in the "Nuclear De-excitation" phase of Figure 1.

5.1.2. BINARY INTRANUCLEAR CASCADE (BIC)

The Binary Intranuclear Cascade model (BIC) simulates p and n-induced cascades below 10 GeV through the propagation of primary nucleons and all secondary particles within a nucleus. It is also capable of simulating π-induced cascades below 1.3 GeV [4]. BIC is based on a detailed 3-dimensional model of the nucleus and exclusively binary scattering between reaction participants and nucleons within the nucleus, making it a hybrid approach that combines both a classical cascade and quantum molecular dynamic (QMD) formalisms [22].

The nucleus is modelled by explicitly positioning nucleons in space and assigning momenta to these nucleons. Each participating nucleon is described as a Gaussian wave package in time, space, and the nucleon's position in configuration and momentum. The total wave function of this system is assumed to be the direct product of the wave functions of the participating nucleons and hadrons. Participating means that they are either primary particles or have been generated/scattered in the process of the cascade [22].

Unlike in QMD where the Hamiltonian can be looked at as self-generating from the system configuration, the Hamiltonian within BIC is calculated from simple, time-independent optical potentials. In addition, only participating hadrons are propagated while nucleons in the nuclear model that are not participating in binary reactions are simply viewed as a representative nucleon configuration. This approach is consistent with the nuclear density distributions, Pauli's exclusion principle, and the total nuclear mass [5, 22].

Propagating particles in the nuclear field is done by numerically solving the equations of motion, using time-independent fields derived from optical potentials. The cascade begins with a projectile and the nuclear description, which terminates when the average energy of all participants within the nuclear boundaries are below a given threshold (approximately > 70 MeV) [22]. The residual participants and the nucleus in its current state are then used to define the initial state of the precompound and nuclear de-excitation models. Unlike the Bertini intranuclear cascade model, BIC does not have its own exclusive precompound and evaporation model sets [5]. BIC instead directly flows into the native precompound, evaporation, and nuclear deexcitation modules of Geant4 that are described below.

5.1.3. LIÈGE INTRANUCLEAR CASCADE MODEL (INCL++)

The Liège Intranuclear Cascade model (INCL++) is a time-like intranuclear cascade model for nucleons and pions that supports interactions of light ions up to A=18 [5, 23]. In pre-collision state, all nucleons within the target nucleus are given position and momentum at random in agreement with Saxon-Woods and Fermi sphere distributions [24, 25]. Both protons and neutrons are moving in a constant potential well describing the nuclear mean field.

At the initial interaction stage the incident particle is given an appropriate energy and impact parameter at random. All nucleons are then set into motion and followed in spacetime. The cascade process involves binary collisions between nucleons, and produced pions, and delta resonances. Particles can be transmitted through or reflected off the surface of the square-well nuclear potentials. Further details on the computational implementations of collision calculations, Pauli blocking, etc., may be found in [23-25]. In the interaction stage the stopping time of the cascade is parametrised (in fm/c) by:

$$t_{stop} = 29.8A_T^{0.16}$$

with A_T being the mass number of the target. At the beginning of the cascade process, the incident particle/ion is located with its own impact parameter on the surface of the "working sphere" that is centred on the target with a radius:

$$R_{max} = R_0 + 8a$$

where R_0 and a are the radius and the diffuseness of the target nucleus density [25]. Particles move in straight-line trajectories between collisions inside the working sphere and are divided into two classifications: participants and spectators. During the defined "stopping time frame", nucleons are constantly moving within each nuclear potential-well with constant depth and a radius which is dependent upon their momentum [24, 25]. If the energy, and in turn the radius, of a given particle exceeds the Fermi energy for that specific nuclear potential-well it is set to equal $R_{max.}$ Participants that leave the working sphere are classified as ejectiles and do not interact anymore, with each cascade ending when either all ejectiles have left the system or "stopping time" is exceeded [24, 25].

INCL++ uses the Geant4 native nuclear deexcitation processes immediately after the cascade stage (it does not include an intermediate pre-equilibrium step) [5]. Alternatively, the ABLA++ model can be used instead by employing the technique outlined in the Geant4 Application Developer Guide (Section "Hadronic Interactions").

5.2. PRECOMPOUND MODEL

The native Geant4 precompound/pre-equilibrium model is considered as an extension to the intranuclear cascade models [4, 5]. It extends the low energy range of the intranuclear cascade models for nucleon-nucleus inelastic collision to provide a "smooth" transition from kinetic stage to the equilibrium stage that feeds into the nuclear deexcitation models. During this time, internal transitions of the pre-compound nuclear system compete with nucleon and light ion cluster emissions [5].

The initial information for calculation of pre-compound nuclear stage consists of the atomic mass number A, charge Z of residual nucleus, its four momentum P_0, excitation energy U, and the number of excitons n. Here n is equal to the sum of the number of particles p (from them p_z are charged) and number of holes h [5]. Through a modified implementation of the Gudima et al.'s semi-classical exciton model [26], with additional corrections outlined [27] and [28], all possible nuclear transitions for the number of excitons n with Δn = +2,−2, 0, are taken into account for emissions of gammas, neutrons, protons, deuterons, tritium and helium nuclei. The passage to the state of statistical equilibrium, which happens when the transition probabilities for increasing and decreasing the exciton number become approximately equal (equilibrium condition), is roughly characterised by an equilibrium number of excitons n_{eq}.

At the end of the pre-equilibrium stage, the residual nucleus is left in an "equilibrium state" where the excitation energy is shared by the entire nuclear system [5]. This equilibrated compound nucleus is characterised by its mass, charge and excitation energy with no further memory of the steps which led to its formation, enabling it to be input into the Geant4 nuclear deexcitation models.

5.3. NUCLEAR DE-EXCITATION

The final de-excitation of a nucleus generated during an intranuclear cascade to a thermalised state can be simulated with several semi-classical models which are responsible for sampling a multiplicity of internal-conversion electrons, neutrons, protons, light ions, isotopes, and photons. Geant4 implements four predominate nuclear de-excitation processes within its reference Physics Lists: evaporation, fission, Fermi-break up, and multi-fragmentation. Through the de-excitation process these four models compete, and in many cases link, with one another until the system reaches a "semi-stable" nuclear state.

5.3.1. NUCLEAR EVAPORATION

At the end of the pre-equilibrium stage, or a thermalising process, the residual nucleus can arrive to an equilibrium state for which the excitation energy E^* is shared between many nucleons. Within Geant4, the emission of particles from such an excited compound nucleus can be modelled as the evaporation of molecules from a fluid via Weisskopf and Ewing's statistical compound nuclear decay formalism [29].

Weisskopf formalism implements a detailed balance principle that relates nuclear transition probabilities from state i to d, and vice versa, through the density of states in each of the two systems:

$$P_{i\to d}\rho(i) = P_{d\to i}\rho(d)$$

where $P_{i\to d}$ is the probability per unit of time of nucleus *d* capturing particle *j* to form compound nucleus *i* which is proportional to the compound nucleus cross-section σ_{inv} [5, 29]. Based on this assumption, the probability that a parent nucleus *i* with an excitation energy *E** emits particle *j* with kinetic energy ϵ in its ground state can be written:

$$P_j(\epsilon)d\epsilon = g_j\sigma_{inv}(\epsilon)\frac{\rho_d(E_{max}-\epsilon)}{\rho_i(E^*)}\epsilon d\epsilon$$

where $\rho_i(E^*)$ is the level density of the evaporating nucleus, $\rho_d(E_{max}-\epsilon)$ is the level density of the daughter (residual) nucleus after emission of a fragment *j*, E_{max} is the maximum energy kinetic energy of the ejectile, and $g_i = \frac{m_j(2s_j+1)}{\pi^2\hbar^2}$ given by the spin (s_j) and the mass (m_j) of the ejectile [5, 29].

The last step of an evaporation cascade consists of the evaporation of photons. Photon evaporation may be simulated as a continuum gamma transition using a dipole approximation or via discrete gamma transitions using an valuated database of nuclear gamma transitions (ENSDF) [30]. The competition between photons and fragments, as well as giant resonance photons, is neglected at this step. Geant4 considers the discrete E0, E1, M1, E2, M2, E3, M3 (including possible mixing) photon transitions from tabulated isotopes. Angular-correlated gamma-emission can be performed (if enabled by the user). The list of isotopes included in the photon evaporation database extends up to A=294, with highest atomic number Z=117 [5]. This database contains experimentally measured excited level energies, spins, parities and relative transitions probabilities. This information is uploaded for Geant4's data libraries on the fly when an excited state is first created during simulation run time.

Float level transition information is also included in ENSDF for a select number of isotopes [30]. This enables the simulation of discrete photon evaporation between floating states of the same floating band. When the lowest floating state of a band is reached the nucleus is set to its ground state [5].

5.3.2. FISSION

The GEANT4 fission model can predict final excited fragments as a result of an excited nucleus, with atomic number *A* ≥ 65, via either symmetric or asymmetric fission. Based on the Bohr and Wheeler theory of fission [31], this model requires that the initial atomic mass number *A*, charge *Z* of excited nucleus, its four momentum P_0 and excitation energy *E** of the mother nuclei be known to simulate the fission decay. Within this model the fission probability (per unit time) W_{fis} is proportional to the nucleon pairing corrected nuclear level density $\rho_{fis}(T)$ [5, 32] at the saddle point:

$$W_{fis} = \frac{1}{2\pi\hbar\rho_{fis}(E^*)}\int_0^{E^*-B_{fis}}\rho_{fis}(E^*-B_{fis}-T)dT$$

$$= \frac{1+(C_f-1)\,exp(C_f)}{4\pi a_{fis}\,exp(2\sqrt{aE^*})}$$

Where B_{fis} is the fission barrier height, $C_f = 2\sqrt{a_{fis}(E^*-B_{fis})}$, and *a* and a_{fis} are the level density parameters of the compound and fission saddle point nuclei respectively [5]. At the saddle point $a_{fis} > a$ with:

- $a_{fis} = 1.08a$ for $Z < 85$,
- $a_{fis} = a[1.04+0.01(89-Z)]$ for $85 \le Z < 89$, and
- $a_{fis} = 1.04a$ $Z \ge 89$.

5.3.3. FERMI-BREAK UP

For a light nucleus with mass number A and charge Z even a relatively small excitation energy may be comparable to its binding energy. In this case it can be assumed that the preferred principal mechanism of de-excitation is the explosive decay of the excited nucleus into several smaller clusters [33]. To describe this process Geant4 implements an updated version of the Femi break-up model applicable to excited nuclei of A < 17 and Z < 9 [4, 5, 34]. This model considers all possible break-up channels which satisfy the mass number, charge, energy and momenta conservations, and considers the competition between these channels. Recently nuclear level energies with this model were changed to match those with in the gamma evaporation database [5].

Within the Geant4 Fermi-break up model a channel will be allowed for decay if the total kinetic energy E_{kin} of all fragments of the given channel at the moment of break-up is positive. This energy can be calculated according to:

$$E_{kin} = U + M(A,Z) - E_{Cou} - \sum_{b=1}^{n}(m_b + \epsilon_b)$$

where *U* the is primary fragment excitation of mass *M(A,Z)*, m_b and ϵ_b are masses and excitation energies of fragments, and E_{Cou} is the Coulomb barrier for a given channel. Here:

$$E_{Cou} = \frac{3e^2}{5r_0}\left(1 + \frac{V}{V_0}\right)^{-1/3}\left(\frac{Z^2}{A^{1/3}} - \sum_{b=1}^{n}\frac{Z^2}{A_b^{1/3}}\right)$$

Where $V_0 = 4\pi r_0^3 A/3$ is the volume of the system corresponding to the normal nuclear matter density for $r_0 = 1.3fm$, and $\frac{V}{V_0} = 6$ is a free parameter of the current Geant4 model [5, 33]. With the total number of possible break-up channels for an excited nucleus known, it's total probability to break-up into *n* components (nucleons, deuterons, tritons, alphas etc) can be determined by:

$$W(E,n) = (V/\Omega)^{n-1}\rho_n(E)$$

where $\rho_n(E)$ is the density of a number of final states, and $\Omega = (2\pi\hbar)^3$ is the normalisation volume. Here $\rho_n(E)$ is dependent on three different factors: phase space, spin, and the permutation of components in the system's final state [5].

5.3.4. MULTI-FRAGMENTATION

The multi-fragmentation model is responsible for explosive break-up of heavier hot nuclei (Z>8, A>16, and excitation energy E>3 MeV/u) [35]. It assumes that an equilibrium between produced fragments is achieved through low-density freeze-out during the expansion phase (i.e. masses and charges of primary fragments are set at the end of this phase). These fragments are then able to interact with other nuclear species through Coulomb and nuclear mean fields during the propagation phase [33]. These interactions can result in their energies and densities being potentially altered. The advantage of the multi-fragmentation model is that all break-up channels of nucleons and excited fragments are considered within the same statistical framework, including the channel corresponding to the formation of a compound nucleus [33]. This enables for a smooth transition between nuclear de-excitation models dependent on the resultant compound nucleus' excitation energy [5].

In the microcanonical treatment the mass *A*, charge *Z*, momentum P_0 and energy *U* of the nuclear system are fixed [33, 36]. It also assumes that the primary fragments are formed in the expanded volume $V > V_0$, where V_0 is the volume at normal nuclear density $\rho_0 = 0.15fm^{-3}$. The probability of a breakup channel *b* of the nuclear system is given by [5, 35]:

$$W_b(U,A,Z) = \frac{exp[S_b(U,A,Z)]}{\sum_b exp[S_b(U,A,Z)]}$$

where $S_b(U, A, Z)$ is the entropy of a multi-fragment state corresponding to the breakup channel *b*. The channels *b* are parametrised relative to their set of fragment multiplicities N_{A_f,Z_f} for each fragment with atomic number A_f and charge Z_f. This requires that all partitions *b* have constraints on the total mass and charge of the nuclear system:

$$\sum_f N_{A_f,Z_f} A_f = A \text{ and } \sum_f N_{A_f,Z_f} Z_f = Z \ .$$

For a detailed review on the "Statistical multifragmentation of nuclei" see [35].

6. RADIOACTIVE DECAY

The native Geant4 radioactive decay process and model handles α, β−, β+, isomeric transition (IT), and electron capture (EC) decays which can be applied to generic ions both in flight and at rest. The simulation model depends on data taken from the Evaluated Nuclear Structure Data File (ENSDF) [30] which provides information on:

- nuclear half-lives,
- nuclear level structure for the parent or daughter nuclide,
- decay branching ratios, and
- the energy of the decay process.

Two major points should be known about the native Geant4 radioactive decay model:

1. Updates to the ENSDF dataset are implemented with every minor Geant4 release (1X.0X), and
2. When daughter nuclei are excited isomers their prompt nuclear de-excitation is treated using Geant4's Photon Evaporation processes (see Nuclear De-excitation) [5].

7. LOW ENERGY NEUTRON PHYSICS PROCESSES/MODELS (> 20 MEV)

As outlined in Section "Hadronic Physics Cross-Section Data", Geant4 possess a set of dedicated low energy neutron physics processes/models (sub 20 MeV) to simulate the transport of neutrons based on the ENDF/B-VI evaluated data library [7]. These low energy neutron transport processes within Geant4, known as NeutronHP, are split into four separate models: elastic scattering, radiative capture, fission, and inelastic scattering. It should be note that all of these models are "**data-driven**" and are based on a combination of experimental or evaluated datasets.

7.1. ELASTIC SCATTERING

The NeutronHP elastic scattering model samples the final system state from normalised differential scattering cross-sections contained in ENDF/B-VI [7]. Depending on the target nuclei this data is tabulated in one of two ways for elastic scattering ENDF/B-VI. The first tabulated dataset is based on linearly interpretable differential cross-sections that are dependent on the cosine of the neutron scattering angle θ and incident kinetic energy *E*:

$$\frac{d\sigma}{d\Omega} = \frac{d\sigma}{d\Omega}(cos\,\theta\,, E)$$

These tabulations are normalised by $\sigma/(2\pi)$ to ensure that the integral of the differential cross-sections with respect to scattering angle yields unity [5]. The second tabulated normalised cross-sectional dataset is represented as a series of Legendre polynomials $P_l(cos\,\theta)$, with the Legendre coefficients a_l tabulated as a function of the incident neutron kinetic energy *E*:

$$\frac{2\pi}{\sigma(E)}\frac{d\sigma}{d\Omega}(cos\,\theta\,, E) = \sum_{l=0}^{n_l} \frac{2l+1}{2} a_l(E) P_l(cos\,\theta)$$

This mixed tabulation style of ENDF/B-VI can be attributed to the fact that it was created using multiple different experimental and evaluated datasets from over 20 different labs across the globe [7].

7.2. RADIATIVE CAPTURE

The photon yields (gamma-rays) from the NeutronHP radiative capture model's final system state is sampled from two tabulated datasets: 1) photon multiplicities, and 2) photon production cross-sections. These nuclei specific tabulated datasets are composed of sub-datasets that contain the discrete and continuous contributions to the emitted photon energy spectra, and their respective angular distributions from ENDF/B-VI.

For a given target nuclei and neutron of incident energy *E,* the discrete photon energy (E_γ) contributions to the emitted photon energy spectra is sampled in a step by step cascade transition manner based on their respective branching probabilities (i.e. identical to the atomic deexcitation process in Geant4) [5, 37]. In the case of the continuum contribution, the normalised emission probability *f* of a photon with energy E_γ is sampled from the weighted sum of normalised distributions *g*:

$$f(E \to E_\gamma) = \sum_i p_i(E) g_i(E \to E_\gamma)$$

where p_i is a function weighted on incident neutron energy. Finally, each emitted photons angular distribution is sampled from either their respective linear interpretable differential cross-sections or Legendre coefficient values in an identical manner to the NeutronHP elastic scattering model [5].

7.3. FISSION

The NeutronHP neutron induced fission model is capable of simulating first chance, second chance, third chance and fourth chance fission. The final system state daughter nuclei and neutron yields for a given target nuclide undergoing fission through one of these four different interaction channels are tabulated as a function of both incoming and outgoing neutron energy. Angular distributions of outgoing daughter nuclei and neutrons are tabulated in the same manner as the NeutronHP elastic scattering: either linear interpretable differential cross-sections or Legendre coefficient values. If ENDF/B-VI lacks the required angular emission data for a given target nuclei, the angular distribution of outgoing daughter nuclei and/or neutrons are simulated as an isotropic source from the systems centre of mass [5]. Further transport modelling of generated "semi-stable" daughter nuclei is handed over to the other hadronic physics processes discussed above.

Six different approaches based on the tabulated datasets which exist within ENDF/B-VI are used to sample the emitted energy spectra of daughter nuclei and neutrons dependent on the target nuclei [7]. The first approach samples the energy distribution of fission neutrons as a normalised function of the incoming and outgoing neutron energy from available tabulated experimental data contained in ENDF/B-VI. This data-driven approach has been shown to yield high precision results, but due to its nature is not available for all potential combinations of incident neutron energy, target nuclei and fission channel. The next three approaches are based on tabulations of different "evaporation" spectra approaches. These are the "general evaporation spectrum":

$$f(E \to E') = f\left(E'/\Theta(E)\right)$$

"Maxwell spectrum":

$$f(E \to E') \propto \sqrt{(\mathrm{E}')} \exp\left(\mathrm{E}'/\Theta(\mathrm{E})\right)$$

and the "evaporation spectrum":

$$f(E \to E') \propto \mathrm{E}' \exp\left(\mathrm{f}\left(\mathrm{E}'/\Theta(\mathrm{E})\right)\right.$$

were *E* is the energy of the incident neutron, *E'* is the energy of a fission neutron, and $\Theta(E)$ is effective temperature used to characterise the secondary neutron energy distribution. For all three "evaporation spectra" approaches the effective temperature and the functional behaviour of the energy distribution are taken from evaluated datasets contained in ENDF/B-VI [7].

The last two approaches are the energy dependent Watt spectrum [38], and the Madland Nix spectrum [39]. For the energy dependent Watt spectrum approach, the fission neutron energy distribution is sampled from:

$$f(E \to E') \propto exp\left(-E'/a(E)\right) sinh\sqrt{b(E)E'}$$

were both *a(E)* and *b(E)* are tabulated as function of incident neutron energy. In the case of the Madland Nix spectrum approach, the fission neutron energy distribution is sampled from:

$$f(E \rightarrow E') = 1/2[g(E', \langle K_l \rangle) + g(E', \langle K_h \rangle)]$$

where:

$$g(E', \langle K \rangle) = \frac{1}{3\sqrt{\langle K \rangle \Theta}}\left[u_2^{3/2}E_1(u_2) - u_1^{3/2}E_1(u_1) + \gamma(3/2, u_2) - \gamma(3/2, u_1)\right],$$

$$u_1(E', \langle K \rangle) = \frac{\left(\sqrt{E'} - \sqrt{\langle K \rangle}\right)^2}{\Theta}, \text{ and}$$

$$u_2(E', \langle K \rangle) = \frac{\left(\sqrt{E'} + \sqrt{\langle K \rangle}\right)^2}{\Theta}.$$

Here K_l is the kinetic energy of light fragments, K_h the kinetic energy of heavy fragments, $E_i(u_i)$ is the exponential integral, and $\gamma(3/2, u_i)$ is the incomplete gamma function. Mean kinetic energies for light ($\langle K_l \rangle$) and heavy ($\langle K_h \rangle$) fragments are assumed to be energy independent, with their values and the incident neutron energy effective temperature Θ of the system sampled from ENDF/B-VI [5, 7].

Finally, any accompanying fission photons emitted during the neutron induced fission process are modelled in similar fashion to those from neutron capture. The emission yields and energies of these fission photons are sampled from evaluated data if available, then the nuclear excitation levels and transition probabilities of ENDF/B-VI [5, 7].

7.4. INELASTIC SCATTERING

NeutronHP inelastic scattering in Geant4 consists of an array of data driven models that encompasses the following incoherent neutron scattering reactions off a target nuclei *A*: (n,nγ) [discrete and continuous γ], (n,np), (n,td), (n,nt), (n,n^{3}He), (n, nα), (n,nd2α), (n,nt2α), (n,n2p), (n,n2α), (n,npα), (n,n3α), (n,2n), (n,2np), (n,2nd), (n,2nα), (n,2n2α), (n,nX), (n,3n), (n,3np), (n,3nα), (n,4n), (n,p), (n,pd), (n,pα), (n,2pd), (n,dα), (n,d2α), (n,dt), (n,t), (n,t2α), (n,^{3}He), (n,α), (n,2α), and (n,3α). Emitted photons (γ) during these inelastic scattering interactions are modelled in an identical manner to those from NeutronHP radiative capture.

When supporting data is present in ENDF/B-VI these data driven models will sample their final system states from isotropic emission, discrete two-body kinematics, N-body phase-space distribution, continuum energy-angle distributions, and continuum angle-energy distributions in the laboratory system tabulations. Otherwise the angular and energy distribution sampling of the final system state products follow a similar process to NeutronHP fusion, with the exception that only the arbitrary tabulation of secondary energies from ENDF/B-VI are utilised [5, 7]. For these instances, if relevant tabulated data is available in ENDF/B-VI, the energy and angular correlated production cross-section for reaction product *K* can be written:

$$\sigma_k(E, E', cos\,\theta) = \sigma(E) Y_K(E) p(E, E', cos\,\theta)$$

where $Y_k(E)$ is the product multiplicity, $\sigma(E)$ is the inelastic cross-section, $p(E, E', cos\,\theta)$ energy and angular depended scattering distribution, and the system is assumed to be azimuthally symmetrical [5]. Of the NeutronHP model set inelastic scattering is the most dependent on the experimental or evaluated datasets contained in ENDF/B-VI, and therefore their accuracy is directly proportional to the available datasets with in ENDF/B-VI.

8. GAMMA-NUCLEAR AND LEPTO-NUCLEAR MODELS

Gamma-nuclear and lepto-nuclear reactions are handled in GEANT4 as hybrid processes which typically require both electromagnetic and hadronic models for their implementation. The following focuses on photonuclear and electronuclear which are required to describe neutron backgrounds and activation in linear colliders. Description of muon-nuclear processes is not covered in this review as their hadronic processes do not become relevant until 10 GeV (see chapter 11 of the Geant4 Physics Reference Manual [5]).

8.1. PHOTONUCLEAR

The photonuclear cross-sections in Geant4 are based on parameterisations that cover all incident photon energies from hadron production threshold upwards [5]. These parameterisations in the sub-GeV energy range can be divided into four energy domains each with their own dominate physical process: Giant Dipole Resonance (GDR) region (< 30 MeV), "quasi-deuteron" region (30 MeV to 150 MeV), Δ isobar region (150 MeV to 450 MeV), and Roper resonance region (450 MeV to 1.2 GeV). Within Geant4 version 10.7, these parameterisations are based on tabulated data of 14 primary nuclei: ^{1}H, ^{2}H, ^{4}He, ^{6}Li, ^{7}Li, ^{9}Be, ^{12}C, ^{16}O, ^{27}Al, ^{40}Ca, Cu, Sn, Pb, and U. The resultant interpolated parameterisations for each energy domain are functions of the target nuclei *A* and $e = log(E_\gamma)$, where E_γ is the incident gamma ray energy [40]. Note that for specific target nuclei addition cross-section data exists that can also be sampled, with about 50 nuclei in total being available over the sub-GeV energy range in Geant4 version 10.7 [5].

In the GDR region (< 30 MeV), the parameterised photonuclear cross-section can be described as the sum of two peaks:

$$\sigma_{GDR}(e) = th(e, b_1, s_1) \cdot exp(c_1 - p_1 \cdot e) + th(e, b_2, s_2) \cdot exp(c_2 - p_2 \cdot e)$$

where the exponential terms represent the falling edge of each resonance peak that is known to have a power law like structure. The nuclear-barrier reflection, and effective resonance threshold, of each resonance peak is represented with:

$$th(e, b_i, s_i) = \frac{1}{1 + exp\left(\frac{b_i - e}{s_i}\right)}$$

where p_1 and p_2 parametrised such that:

$p_1 = 1, p_2 = 2$ for	$A < 4$
$p_1 = 2, p_2 = 4$ for	$4 \leq A < 8$
$p_1 = 3, p_2 = 6$ for	$8 \leq A \leq 12$
$p_1 = 4, p_2 = 8$ for	$A \geq 12$

with b_i, c_i and s_i parameterise for a given target nuclei *A* [5, 40].

For the "quasi-deuteron" region (30 MeV to 150 MeV):

$$\sigma_{QD}(e, v, w, u) = \frac{v}{1 + w \cdot (e - u)^2}$$

In the case of ^{1}H and ^{2}H, the quasi-deuteron contribution is almost zero and their parameters are adjusted to use their third baryonic resonance cross-sections [40]. The following outlines the relationship of these parameters as a function of the target nuclei *A*:

- $v = \frac{exp(-1.7 + a \cdot 0.84)}{1 + exp(7 \cdot (2.38 - a))}$ where $a = log(A)$ (with v = 0.078 for ^{1}H, and v = 0.08 for ^{2}H), and
- u = 3.7 and w = 0.4 which is set to be static due to the lack of experimental data to determine their target nuclei A dependence (with u = 6.93 and w = 90 for both ^{1}H and ^{2}H)

Parameterisation of the Δ isobar region (150 MeV to 450 MeV) is similar to that of the quasi-deuteron contribution with the addition of the threshold function *th*:

$$\sigma_\Delta(e, d, f, g, r, q) = \frac{d \cdot th(e, f, g)}{1 + r \cdot (e - q)^2}$$

where *d* is an overall normalisation factor, *q* can be interpreted as the energy of the Δ isobar, and *r* the inverse Δ width. The following outlines the relationship of these parameters as a function of the target nuclei *A*:

- $d = 0.41 \cdot A$ (i.e. σ_Δ is proportional to A) with special case ^{1}H = 0.55 and ^{2}H = 0.88,
- $f = 5.13 - 0.00075 \cdot A$,

- g = 0.09 for $A \geq 7$ and 0.04 for $A < 7$,
- q = 5.84 - $\frac{0.09}{1+0.003 \cdot A^2}$, and
- r = 11.9 – 1.24 · $log(A)$ (with r=18.0 for ^{1}H) [40].

The Roper resonance region cross-section (450 MeV to 1.2 GeV) was parameterised in the same form as the quasi-deuteron contribution:

$$\sigma_{Tr}(e, v, w, u) = \frac{u}{1 + w \cdot (e - u)^2}$$

where $a = log(A)$ and the parameter values are:

- $v = exp(a \cdot 0.84 - 2)$ (with v = 0.22 for ^{1}H and v = 0.34 for ^{2}H),
- $u = 6.46 + a \cdot 0.061$ (with u = 6.57 for ^{1}H and ^{2}H), and
- $w = 0.1 + a \cdot 1.65$ (with w = 20 for ^{1}H and w = 15 for ^{2}H).

Finally, it should be noted that with the release of Geant4 version 11 a new set of photonuclear models will be released. At the time of writing this report there is limited information regarding this new model set, however it is known that it will be data-driven based on the 2019 IAEA evaluated photonuclear data library [41].

8.2. ELECTRONUCLEAR

Electronuclear interactions are closely connected with photonuclear interactions and are sometimes even referred to as a subset due to the dominate role that the one-photon exchange mechanisms play [42]. Geant4 uses a variant of the Equivalent Photon Approximation (EPA) that approximates electronuclear scattering cross-sections in terms of a flux of equivalent photons interacting with a target nuclei A [5, 40]. This formalism factorises the equivalent photon flux contributions into their real transversely (σ_T) and their virtual longitudinally (σ_L) polarised components to enable the differential electronuclear scattering cross-section to be written:

$$\frac{d^2\sigma}{dydQ^2} = \frac{\alpha}{\pi Q^2}(S_{TL} \cdot (\sigma_T + \sigma_L) - S_L \cdot \sigma_L)$$

where:

$$S_{TL} = y\frac{1 - y + \frac{y^2}{2} + \frac{Q^2}{4E^2} - \frac{m_e^2}{Q^2}\left(y^2 + \frac{Q^2}{E^2}\right)}{y^2 + \frac{Q^2}{E^2}}$$

$$S_L = \frac{y}{2}\left(1 + \frac{2m_e^2}{Q^2}\right)$$

E is the energy of the incident particle, Q^2 is the invariant square of the momentum transfer to the nucleus, $\alpha = e^2/4$, and m_e is the mass of an electron. Further details outlining the Geant4 electronuclear scattering model's behaviour as a factor of target nuclei A and momentum transfer to the nucleus can be found in [5, 40, 42].

9. REFERENCES

[1] Geant4 Collaboration (1998), *GEANT4: An object-oriented toolkit for simulation in HEP*, CERN Report CERN/LHCC 98-44.

[2] Agostinelli S. et al. (2003), *GEANT4—a simulation toolkit*, Nuclear Instruments and Methods in Physics Research Section A 506(3): 250-303.

[3] Allison J. et al. (2006), *Geant4 developments and* applications, IEEE Transactions on Nuclear Science 53(1): 270-278.

[4] Allison J. et al. (2016), *Recent developments in Geant4,* Nuclear Instruments and Methods in Physics Research Section A 835: 186-225.

[5] Geant4 Collaboration (2021), *GEANT4 Physics Reference Manual - Version 10.7*, https://geant4.web.cern.ch .

[6] Particle Data Group (2016), *Review of particle physics*, Chinese Physics C 40(10): 100001.

[7] Rose P. F. (1991) *ENDF-201: ENDF/B-VI summary documentation,* (No. BNL-NCS-17541; ENDF-201) Brookhaven National Lab.

[8] Barashenkov V. S. (1989), *Nucleon-nucleus cross sections*, (No. JINR-R--2-89-770) Joint Inst. for Nuclear Research.

[9] Barashenkov V. S. and Toneev V.D. (1972), Interactions of high energy particles and atomic nuclei with nuclei; Vzaimodeistviya vysokoenergeticheskikh chastits i atomnykh yader s yadrami.

[10] Grichine V. M. (2009), *A simple model for integral hadron–nucleus and nucleus–nucleus cross-sections*, Nuclear Instruments and Methods in Physics Research Section B 267(14): 2460-2462.

[11] Grichine V. M. (2009), *A simplified Glauber model for hadron–nucleus cross sections*, The European Physical Journal C 62(2): 399-404.

[12] Barshay S., Dover C. B. and Vary J. P. (1974), *The validity of the factorization hypothesis for nucleus-nucleus cross sections at high energies*, Physics Letters B 51(1): 5-8.

[13] Barshay S., Dover C. B. and Vary J. P. (1975), *Nucleus-nucleus cross sections and the validity of the factorization hypothesis at intermediate and high energies*, Physical Review C 11(2): 360.

[14] Sihver L., Tsao C. H., Silberberg R., Kanai T. and Barghouty A. F. (1993*), Total reaction and partial cross section calculations in proton-nucleus ($Z_t \leq 26$) and nucleus-nucleus reactions (Z_p and $Z_t \leq 26$)*, Physical Review C 47(3): 1225.

[15] Shen W. Q., Wang B., Feng J., Zhan W. L., Zhu Y. T. and Feng E. P. (1989), *Total reaction cross section for heavy-ion collisions and its relation to the neutron excess degree of freedom*, Nuclear Physics A 491(1): 130-146.

[16] Wright D. H. and Kelsey M. H. (2015), *The Geant4 Bertini cascade*, Nuclear Instruments and Methods in Physics Research Section A 804:175-188.

[17] Griffin J. J. (1966), *Statistical model of intermediate structure*, Physical Review Letters 17(9): 478.

[18] Griffin J. J. (1967), *Energy dependence of average direct reaction cross sections and partial nuclear level densities*, Physics Letters B 24(1): 5-7.

[19] Dostrovsky I., Fraenkel Z. and Friedlander G. (1959), *Monte Carlo calculations of nuclear evaporation processes. III. Applications to low-energy reactions*., Physical Review 116(3): 683.

[20] Dostrovsky I., Fraenkel Z. and Rabinowitz P. (1960), *Monte Carlo calculations of nuclear evaporation processes. V. Emission of particles heavier than He 4*, Physical Review 118(3): 791.

[21] Weisskopf V. (1937), *Statistics and nuclear reactions*, Physical Review 52(4): 295.

[22] Folger G., Ivanchenko V. N. and Wellisch J. P. (2004), *The binary cascade*, The European Physical Journal A 21(3): 407-417.

[23] Mancusi D., Boudard A., Cugnon J., David J. C., Kaitaniemi P. and Leray S. (2014), *Extension of the Liège intranuclear-cascade model to reactions induced by light nuclei*, Physical Review C 90(5): 054602.

[24] Boudard A., Cugnon J., Leray S. and Volant C. (2002), *Intranuclear cascade model for a comprehensive description of spallation reaction data*, Physical Review C 66(4): 044615.

[25] Boudard A., Cugnon J., David J. C., Leray S. and Mancusi D. (2013), *New potentialities of the Liège intranuclear cascade model for reactions induced by nucleons and light charged particles*, Physical Review C 87(1): 014606.

[26] Gudima K. K., Mashnik S. G. and Toneev V. D. (1983), *Cascade-exciton model of nuclear reactions*, Nuclear Physics A 401(2): 329-361.

[27] Apostolakis J. et al. (2009), *Progress in hadronic physics modelling in Geant4*, Journal of Physics (Conference Series) 160(1): 012073.

[28] Ivantchenko A. V., Ivanchenko V. N., Molina J. M. Q. and Incerti S. (2012), *Geant4 hadronic physics for space radiation environment*, International Journal of Radiation Biology 88(1-2): 171-175.

[29] Weisskopf V. F. and Ewing D. H. (1940), *On the yield of nuclear reactions with heavy elements*, Physical Review 57(6): 472.

[30] Bhat M. R. (1992), *Evaluated nuclear structure data file (ENSDF)*, Nuclear Data for Science and Technology: 817-821.

[31] Bohr N. and Wheeler J. A. (1939), *The mechanism of nuclear fission*, Physical Review 56(5): 426.

[32] Hurwitz H. (Jr.) and Bethe H. A. (1951), *Neutron capture cross sections and level density*, Physical Review 81(5): 898.

[33] Pshenichnov I., Botvina A., Mishustin I. and Greiner W. (2010), *Nuclear fragmentation reactions in extended media studied with Geant4 toolkit*, Nuclear Instruments and Methods in Physics Research Section B 268(6): 604-615.

[34] Fermi E. (1950), *High energy nuclear events*, Progress of Theoretical Physics 5(4): 570-583.

[35] Bondorf J. P., Botvina A. S., Iljinov A. S., Mishustin I. N. and Sneppen K. (1995), *Statistical multifragmentation of nuclei*, Physics Reports 257(3): 133-221.

[36] Botvina A.S. and Mishustin I.N. (2001), *Statistical evolution of isotope composition of nuclear fragments*, Physical Review C 63(6): 061601.

[37] Incerti S. et al. (2016), *Simulation of Auger electron emission from nanometer-size gold targets using the Geant4 Monte Carlo simulation toolkit*, Nuclear Instruments and Methods in Physics Research Section B 372: 91-101.

[38] Watt B. E. (1952), *Energy spectrum of neutrons from thermal fission of U 235*, Physical Review 87(6): 1037.

[39] Madland D. G. and Nix J. R. (1982), *New calculation of prompt fission neutron spectra and average prompt neutron multiplicities*, Nuclear Science and Engineering 81(2): 213-271.

[40] Wellisch J. P., Kossov M. and Degtyarenko P. (2003), *Electro and gamma nuclear physics in Geant4*, arXiv:nucl-th/0306012.

[41] Kawano T., et al. (2020), *IAEA photonuclear data library 2019*, Nuclear Data Sheets 163: 109-162.

[42] Pomeranchuk I.Y. and Shumushkevich I.M. (1961), *On processes in the interaction of γ-quanta with unstable particles*, Nuclear Physics 23: 452-467.

10. REVISION HISTORY

Document No:		ADI-ERP-2022-002	
Document Title:		A CONDENSED OVERVIEW OF SUB-GEV HADRONIC PHYSICS IN GEANT4	
Revision	Description	Prepared by	Reviewed by
1	Original Issue	J M C Brown	A Flynn
2	Release version	J M C Brown	D Boardman
3	Release updated version	J M C Brown	A Flynn